Effects of Si surficial structure on transport properties of $La_{2/3}Sr_{1/3}MnO_3$ films*

Xiao-Min Gu(顾晓敏)[1], Wei Wang(王伟)[2], Guo-Tai Zhou(周国泰)[1], Kai-Ge Gao(高凯歌)[1], Hong-Ling Cai(蔡宏灵)[1], Feng-Ming Zhang(张凤鸣)[1], and Xiao-Shan Wu (吴小山)[1,†]

[1] *Collaborative Innovation Center of Advanced Microstructures, Laboratory of Solid State Microstructures, Photovoltaic Engineering Center, School of Physics, Nanjing University, Nanjing* 210093, *China*

[2] *Collaborative Innovation Center of Advanced Microstructures, Laboratory of Solid State Microstructures, School of Electronic Science and Engineering, Nanjing University, Nanjing* 210093, *China*

(Received 24 March 2016; revised manuscript received 25 May 2016; published online 25 August 2016)

$La_{2/3}Sr_{1/3}MnO_3$ films are deposited on (001) silicon substrates, in which the silicon surfaces have artificially been treated into the scallops-like, pyramid-like, and smooth polishing structure, by pulsed laser deposition. The magnetoresistances of the films on etched substrates under low applied field are very sensitive to the applied field, and much larger (14.3% for acid-etched, and 42.9% for alkali-etched) than that on the polished Si at 5 K. Zero-field-cooled and field-cooled magnetization behaviors are measured and analyzed. Remarkable upturn behaviors in temperature-dependent resistivity for all samples are observed at low temperature, which follows the Efros–Shkloskii variable range hopping law and the Arrhenius law. We believe that the rough surface may be useful in device design.

Keywords: $La_{2/3}Sr_{1/3}MnO_3$ film, silicon, microstructure, magnetoresistance

PACS: 67.25.dp, 73.43.Qt, 77.55.df, 81.65.Cf **DOI:** 10.1088/1674-1056/25/10/106701

1. Introduction

Transition metal oxides, strongly correlated electron systems, have a variety of interesting electronic and magnetic properties because of the strong coupling between spin, charge and orbital degree of freedom.[1,2] In particular, perovskite manganite ($Re_{1-x}Ae_xMnO_3$, Re = rare earth element, Ae = alkaline earth element) as a functional oxide has attracted a great deal of attention since the discovery of colossal magnetoresistivity (CMR)[3,4] due to their potential applications in spintronics.[5–7] In recent years, manganite-based heterojunctions[8–14] have received a great deal of attention since fancy properties could be aroused by the interfacial effect. Among the variable manganites, the hole-doped (p-type) $La_{2/3}Sr_{1/3}MnO_3$ (LSMO) is considered as one of the most promising candidates for applications because of its high Curie temperature ($T_C \approx 360$ K) and high spin polarization (100%).[1] $SrTiO_3$, Nb-doped $SrTiO_3$, and silicon are the most commonly used N-zone materials to form the manganite-based heterojunctions. As a traditional semiconductor, silicon has been the most fundamental technological material in the electronics industry up to now. It is more economical and easier to manipulate than $SrTiO_3$ and Nb-doped $SrTiO_3$, so the fabrication of manganite with silicon-based spintronic devices is a great step to realize their commercial applications. Integrating LSMO thin films and nanostructures on silicon or on silicon with nanostructure is the major patterns. For example, depositing LSMO thin film on Si nanotips is found to be an effective approach to enhancing the electron injection effect.[15,16] In the present work, silicon wafers with micron-scale surface structures are obtained by the wet etching process which is commonly used in solar cell manufacture to form LSMO–silicon heterojunctions and explore the electronic and magnetic properties of LSMO films on different silicon substrates with micro-structures. Low field magnetoresistance is greatly enhanced for films on the etched substrates.

2. Experiments

Elliptical scallops-like texture on (001) silicon single crystal is etched by mixing acid (with volume ratio of 25:6:17 for nitric acid (70%), hydrofluoric acid (40%), and deionized water, respectively) for 6 min at 8 °C[17] (called acid-etched substrate). A pyramid-like texture on the same (001) Si wafer is etched by dilute sodium (sodium hydroxide 2%, nonahydrate sodium silicate 1.3%, isopropanol l6%, deionized water 90.7%) for 15 min at 80 °C (named alkali-etched substrate). For sodium etch, considering the volatility of isopropanol, it is added into the reaction liquid right before the etching process. Before film deposition, the oxide layer on silicon substrate is etched by 10% HF solution for 10 s. $La_{2/3}Sr_{1/3}MnO_3$ (LSMO) thin films are then deposited by pulsed laser deposition (PLD)[18] on the polished silicon wafer (the film is denoted as s1), acid-etched silicon wafer (the film is denoted as s2), and alkali-etched silicon wafer (the film is denoted as s3) at a temperature of 850 °C under an oxygen pressure of

*Project supported by the National Natural Science Foundation of China (Grant Nos. U1332205, 11274153, 11204124, and 51202108).

†Corresponding author. E-mail: xswu@nju.edu.cn

© 2016 Chinese Physical Society and IOP Publishing Ltd

10 mbar (10 bar = 10^5 Pa) for 20 min each, in which case we believe that the films are nearly the same in thickness. The frequency of the laser pulse is 4 Hz. After the deposition, the films are annealed at 800 °C for 2 h in oxygen gas atmosphere. The structures of Si substrates and LSMO/Si at room temperature are characterized by x-ray diffraction (XRD) which is performed in a Rigaku Dmax/rb diffractometer using a Cu K_α source (with an average wavelength of $\lambda_{K\alpha} = 1.5418$ Å). A step scanning mode with the step size of 0.02° in delta (2θ) and integration time of 1 s is used during the collection of XRD data. The surface morphologies of silicon wafers and the LSMO films are observed by atomic force microscope (AFM) and scanning electron microscope (SEM). Transmission electron microscopy (TEM) is used to measure the thickness values and crystalline states of the films. Magnetizations of the films are measured by using a superconducting quantum interference device (SQUID). The magnetic field and temperature dependence of the resistivity are measured in a physical property measurement system (PPMS) by the standard four-probe technique at a temperature range from 1.9 K to 400 K.

3. Results and discussion

LSMO is of pseudocubic structure with lattice parameter $a_{LSMO} = 3.873$ Å.[19–21] It could also be considered as a tetragonal structure whose in-plane basis vectors are rotated 45° with respect to that of the pseudocubic structure. Hence the in-plane lattice parameter of tetragonal structure is $a'_{LSMO} = \sqrt{2}a_{LSMO} = 5.477$ Å, which is quite close to the lattice parameter of single crystal silicon ($a_{Si} = 5.431$ Å). Then the lattice mismatch between substrate and the film is $\delta = (a_{Si} - a'_{LSMO})/a_{Si} = -0.86\%$, which is rather small. Hence we hope that the LSMO thin films on polished silicon (s1) are highly oriented epitaxial films. But as shown in Fig. 1, the XRD pattern of LSMO thin film of s1 demonstrates a polycrystalline film with LSMO rhombohedral phase, not the epitaxial film as expected. The XRD patterns of s2 and s3 show only weak diffraction peaks at (110)/(104), (024), and (018) of LSMO poly-crystal. In addition, amorphous-like bumps of LSMO near (110)/(104) and obvious SiO_2 diffraction peaks also arise. Therefore, we believe that poly-crystal combined with amorphous LSMO films are formed on etched substrates (s2 and s3).

The AFM image of the surface on s1 is shown in Fig. 2(a), which indicates that s1 has a relatively smooth surface, and its roughness is 1.1 nm. We also perform a cross section TEM measurement for s1 as presented in Fig. 2(b). Although the de-oxidation is carried out for Si wafer before being placed into the vacuum chamber, an oxidization layer on the silicon with a thickness of 13.8 nm is observed, which may result from the oxygen atmosphere and form the interlayer between LSMO and Si. The oxidization may prevent the LSMO film from epitaxially growing on silicon, hence the polycrystalline develops. So epitaxially growing functional oxide on silicon is quite tough since one must make sure the sample chamber is in a high vacuum when the substrate is heated and then in oxygen during the deposition. Zhou *et al.* have obtained epitaxial $SrTiO_3$ thin film on silicon with the help of a interlayer of Sr by laser molecular beam epitaxy (MBE).[22] But a direct deposition of functional oxide on silicon by PLD has not been reported. Figures 2(c) and 2(d) show the SEM images of the acid-etched and alkali-etched substrates, which have the textures of micronscale elliptical scallops and pyramids with the sizes of about 4 μm–10 μm and 2 μm–10 μm, respectively. The formation of the pyramid-like texture is due to the anisotropy of the etching caused by sodium hydroxide, which corrodes a series of crystal planes and keeps ⟨111⟩ planes that have the largest atomic density.[23–25] The erosion created by hydrofluoric acid is almost isotropic, hence the surface after erosion does not have a definite crystal orientation. The silicon after wet etching is usually more active, which may be the reason why more obvious SiO_2 diffraction peaks emerge in Figs. 1(b) and 1(c). As the thickness of film is quite small compared with the scale of scallops-like and pyramid-like texture, the morphologies of s2 and s3 are almost the same as those of their substrates. Although alkali-etched substrate has obtained ⟨111⟩ planes, the etched surface is not smooth on each crystal plane which may have a large number of defects (see the inset of Fig. 2(d)), neither is the surface of acid-etched substrate as presented in the inset of Fig. 2(c). During a film deposition, the adatoms diffuse between adsorption sites of different depths on the surface. With different atomic structures and chemistries, the surface shows different potential energy landscapes in the eyes of the adatoms. The diffusion coefficient or diffusivity is expressed as

$$D = D_0 \, e^{-E_d/k_B T}, \tag{1}$$

where E_d represents the diffusion barrier,[26] k_B is the Boltzmann constant, and D_0 is a parameter in relation to the distance between the absorption sites and attempt frequency. Apparently, larger diffusion barrier E_d possessed by etched silicon will result in a smaller diffusion rate. Hence lots of adatoms are localized at the defects as they are difficult to diffuse on the surface. Then the probability of collision nucleation caused by adatom diffusion is reduced, thereby the crystal nucleus is hard to grow up. On the other hand, a large number of adatoms accumulate at defects rapidly without fully crystalizing. Thus the amorphous-additional poly-crystal films with smaller grain sizes are formed on etched silicon substrates.

Figure 3 shows the plots of field-cooled (FC) and zero-field-cooled (ZFC) magnetization versus temperature in a range from 5 K to 400 K with an applied field of $H = 500$ Oe (1 Oe = 79.5775 A·m^{-1}) parallel to the film surface. The values of Curie temperature T_C for s1, s2, and s3 are 322 K,

295 K, and 335 K, respectively. FC and ZFC bifurcation are observed at low temperature for all samples, indicating a spin-glass-like behavior with freezing temperature T_f values of 59 K (s1), 105 K (s2), and 120 K (s3),[27] respectively. The inset in Fig. 3 shows the magnetic hysteresis loops at 5 K. The magnetization curves and hysteresis loops both indicate that each of the films on etched substrates has a weaker magnetism than that on the polished one. The hysteresis loops demonstrate that magnetic easy axes of s2 and s3 rotate to the out-plane direction compared with s1 which has an in-plane easy axis. Actually, the films of s2 and s3 can be divided into lots of tiny film planes which also have their own in-plane easy axes, so the whole magnetization of film would be a vector sum of tiny film planes. As the magnetic moments of tiny film planes of s2 and s3, each has an out-of-plane component, the weaker magnetization and rotation of easy axis would be inevitable.

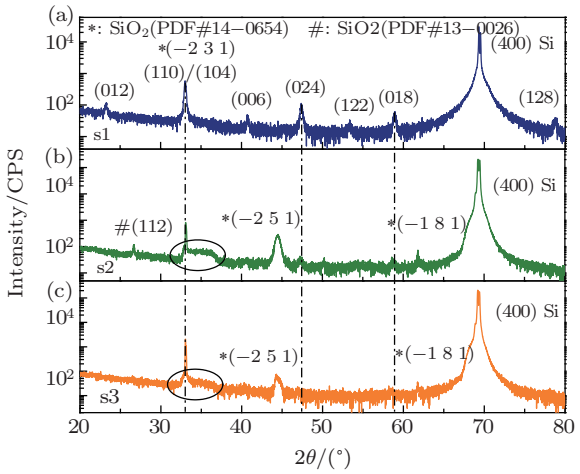


Fig. 1. (color online) X-ray diffraction patterns at room temperature with a wavelength of 1.5418 Å. Peaks marked with * and # belong to SiO_2 layers formed between LSMO and Si. The bumps near (110)/(104) of LSMO may indicate the amorphous structures grown in s2 and s3.

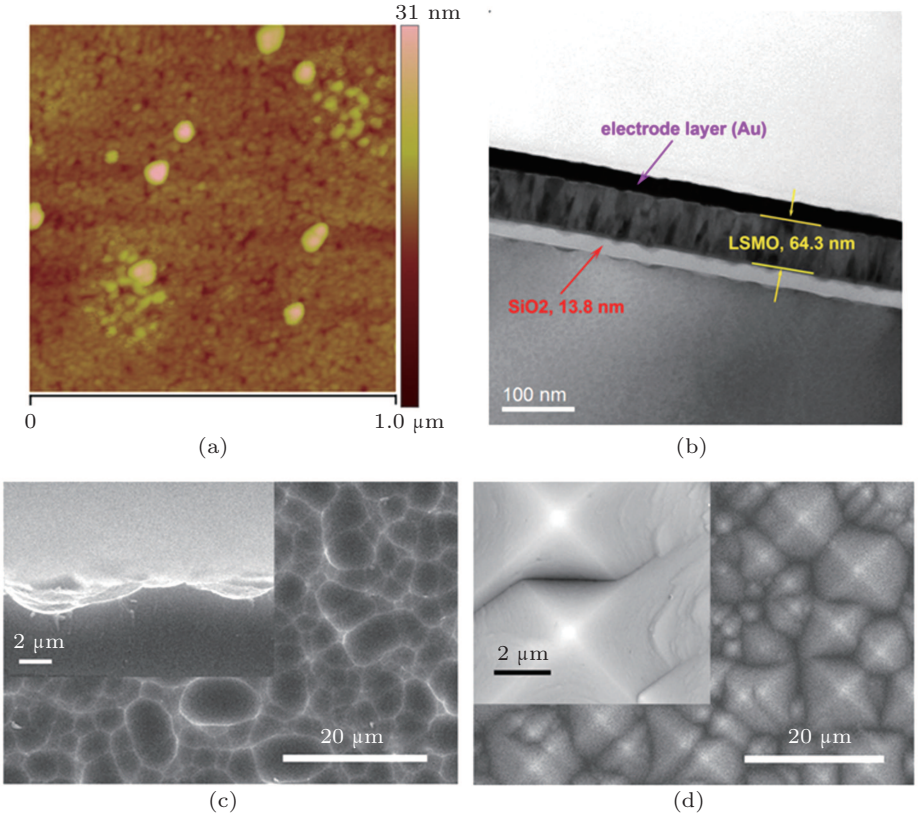


Fig. 2. (color online) (a) AFM image of the surface of s1; (b) the cross section TEM image of s1; SEM images of (c) s2, and (d) s3 substrate.

The temperature-dependent resistivities in a temperature range between 1.9 K and 400 K are shown in Fig. 4(a). The resistivity has a very broad metal-insulator transition and a steep upturn under low temperature.[28,29] In general, there are three kinds of usual mechanisms for the resistivity upturn at low temperature. The Kondo effect caused by the scattering of electrons due to magnetic impurities is eliminated immediately as there is no linearity between the measured resistivity and $\ln T$ in the upturn range (shown in Fig. 4(b)).[28,29] Another explanation for resistivity upturn or minimum is to introduce the concept of quantum correction to conductivity (QCC).[30] While the QCC theory fits the bulk material, and it should be used carefully for polycrystalline samples, for it might be masked by grain boundary effects. According to the following analysis, grain boundary effects are the exact cause of resistivity upturn in the low temperature range. The temperature dependence of resistivity may be fitted based on Efros–Shklovskii variable range hopping (ES-VRH) ($\rho = \rho_0 \exp(T_0/T)^{1/2}$)[31–36] for sample s1, and Arrhenius law ($\rho = \rho_0 \exp(T_0/T)$) for samples s2 and s3, where pa-

rameter T_0 is a characteristic temperature signifying the impurity disorder in the system, and ρ_0 is the residual resistivity. The variable range hopping (VRH) is generally described as $\rho = \rho_0 \exp(T_0/T)^p$, where $p = 1/(d+1)$. Parameter d represents the dimension of the system, so $p = 1/2$, 1/3, and 1/4 correspond to 1 dimension, 2 dimensions, and 3 dimensions, respectively.

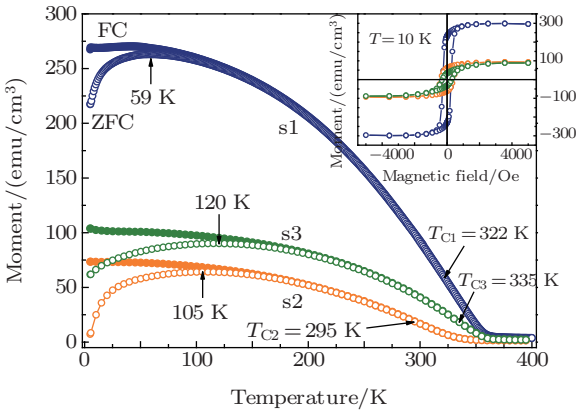


Fig. 3. (color online) Plots of field-cooled (FC) and zero-field-cooled (ZFC) magnetization versus temperature in a range from 5 K to 400 K, with the applied field being 500 Oe parallel to the film surface. The inset shows the hysteresis loops at 5 K.

The Arrhenius law is a hopping model with constant hopping length. According to the above analysis, it seems that s1 is a one-dimensional (1D) system. However, as polycrystalline, s1 is definitely a three-dimensional (3D) system whose resistivity should obey the Mott VRH with $p = 1/4$. The reason why s1's resistivity obeys Efos–Shklovskii-VRH rather than Mott-VRH is the existence of the Coulomb gap in polycrystalline s1.[31,32]

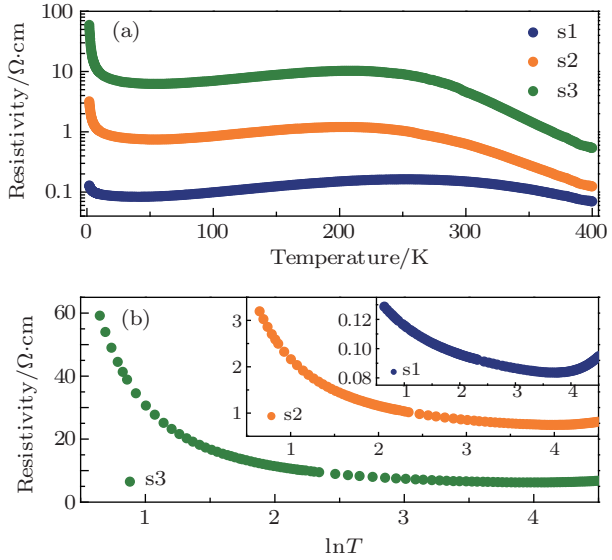


Fig. 4. (color online) (a) The temperature-dependent resistivity from 1.9 K to 400 K, (b) resistivity verses ln$T$ curves for the three samples. If the resistivity obeys the Kondo effect law, the curves would be straight lines.

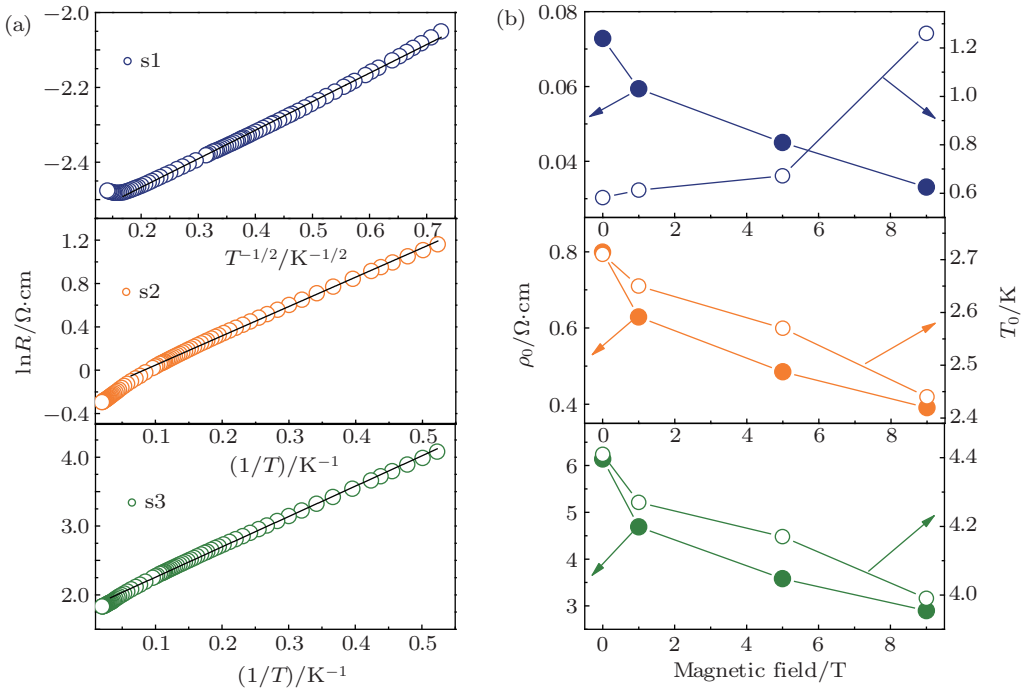


Fig. 5. (color online) Plots of linear fittings ln$R$–$T^{-1/2}$ for s1; ln$R \sim T^{-1}$ for s2 and s3 of three samples at low temperatures. (b) Variations of fitted residual resistance ρ_0 and characteristic temperature T_0 with magnetic field.

In the VRH model, there is a fundamental assumption: the hopping length r^* should be greater than the single grain size a. The characteristic length $r^*(T)$ is given by

$$r^*(T) = \sqrt{\frac{e^2 \xi a}{2T\tilde{\kappa}}}, \qquad (2)$$

where ξ is the dimensionless localization length which decreases with increasing temperature, and $\tilde{\kappa}$ is the effective dielectric constant of a granular sample.[37] When the hopping length is on the order of grain size $r^*(T') \sim a$ at temperature T', the VRH picture will no longer be suitable because the

hopping exists only between adjacent grains. So at this point, a crossover from Efros–Shklovskii VRH to Arrhenius law usually happens.[38] As shown in Fig. 6, this phenomenon exists in s1, where the crossover happens at about 15 K. According to this phenomenon, we speculate that the sizes of grains in s2 and s3 are smaller than in s1, which are similar to the weak diffraction peaks in Figs. 1(b) and 1(c).

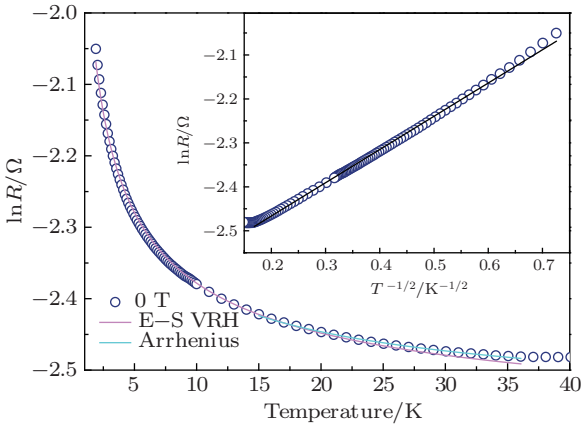


Fig. 6. (color online) Crossover from E–S VRH to Arrhenius law in s1, with the inset showing the linear fitting of $\ln R$ versus $T^{-1/2}$.

The same fittings are also implemented with applied magnetic fields of 1 T, 5 T, and 9 T. The fitted residual resistance ρ_0 and characteristic temperature T_0 each as a function of applied field are shown in Fig. 5(b). All the three ρ values gradually decrease with increasing magnetic field, indicating the negative magnetoresistance (MR). In Efros–Shklovskii VRH law, the relation between the characteristic temperature and the localization length is $T_0 \sim e^2/a\tilde{\kappa}\xi$. So the localization length ξ has the opposite trend to T_0, which decreases with increasing applied field, meaning that the magnetic field aggravates the localization of electrons to a certain degree in s1. That is to say the magnetic field has two opposite effects on the conductivity of s1: on the one hand it increases the conductivity by reducing the residual resistance ρ_0, on the other hand it also reduces the conductivity by aggravating the localization of electrons. While for the Arrhenius behaviors in s2 and s3, the activation energy is given by

$$U = k_B T_0, \tag{3}$$

where k_B is the Boltzmann constant and T_0 is the characteristic temperature.[37] T_0 decreases with increasing magnetic field, so does the activation energy, which means that the activations of electrons become easier with the increase of applied field.

We also measure the *MR–H* hysteresis loops between −5000 Oe and 5000 Oe at 5 K. Here, the *MR* ratio is defined as

$$MR = \frac{R(H) - R(5000\ \text{Oe})}{R(5000\ \text{Oe})} \times 100\%. \tag{4}$$

The *MR–H* loops at 5 K are shown in Fig. 7, in which peaks obviously turn up for all samples at about 550 Oe and s3 has the sharpest peaks. The peak values of 28%, 32%, and 40% are obtained for s1, s2, and s3, respectively. In other words, films on etched silicon wafers have a more sensitive response to an applied magnetic field, which may be valuable for their applications in memory devices or sensitive devices. As these two films are amorphous-additional polycrystals, there are more disordered spin orientation distributions, which is in consistent with our previous analysis in low temperature-dependent resistivity. Hence the effects of applied magnetic field in s2 and s3 are more remarkable than in s1.

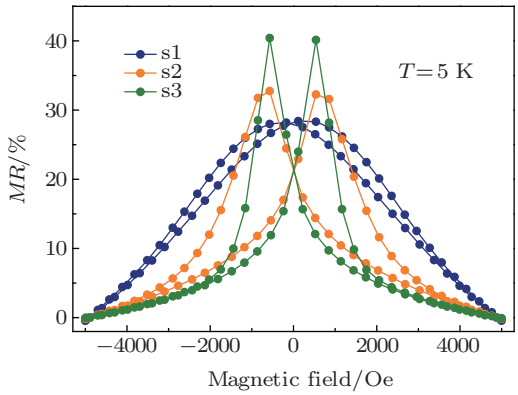


Fig. 7. (color online) Plots of magnetoresistance (*MR*)–*H* loops at 5 K. The peak values of 28%, 32%, and 40% are obtained for s1, s2, and s3, respectively.

4. Conclusions

$La_{2/3}Sr_{1/3}MnO_3$ films are deposited on (001) single crystal silicon wafers with different morphologies, which are polished plane, with elliptical scallops-like texture and pyramid-like texture, respectively. The structures, morphologies, magnetisms and electromagnetic transportation properties are detected. The textures on etched silicon wafers make the films deposited on them amorphous-additional polycrystal rather than pure polycrystalline as deposited on the unetched wafer. The magnetism is weakened, so is the electrical conductivity. Efros–Shklovskii variable range hopping (s1) and Arrhenius law (s2 and s3) show the behaviors of resistivity at low temperature. Sharp peaks are detected in *MR–H* hysteresis loops with peak values of 28%, 32%, and 40%, respectively. It means that the texture causes a more sensitive response to the applied magnetic field in film, which may be valuable for its applications in memory devices or sensitive devices.

References

[1] Moreo A, Yunoki S and Dagotto E 1999 *Science* **283** 2034
[2] Takagi H and Hwang H Y 2010 *Science* **327** 1601
[3] Jin S Tiefel T H, McCormack M, Fastnacht R A, Ramesh R and Chen L H 1994 *Science* **264** 413
[4] Guo X, Dai S, Zhou Y, Yang G and Chen Z 1999 *Appl. Phys. Lett.* **75** 3378
[5] Garcia V Bibes M, Bocher L, Valencia S, Kronast F, Crassous A, Moya X, Enouz-Vedrenne S, Gloter A, Imhoff D, Deranlot C, Mathur N D, Fusil S, Bouzehouane K and Barthélémy A 2010 *Science* **327** 1106
[6] Prezioso M, Riminucci A, Bergenti I, Graziosi P, Brunel D and Dediu V A 2011 *Adv. Mater.* **23** 1371

[7] Sultan K, Ikram M, Gautam S, Lee H K, Chae K H and Asokan K 2015 *RSC Adv.* **5** 69075
[8] Tanaka H, Zhang J and Kawai T 2001 *Phys. Rev. Lett.* **88** 027204
[9] Jin K j, Lu H B, Zhao K, Ge C, He M and Yang G Z 2009 *Adv. Mater.* **21** 4636
[10] Chattopadhyay S and Nath T K 2011 *Curr. Appl. Phys.* **11** 1153
[11] Wang C, Jin K J, Zhao R Q, Lu H B, Guo H Z, Ge C, He M, Wang C and Yang G Z 2011 *Appl. Phys. Lett.* **98** 181101
[12] Yada H Matsubara M, Yamada H, Sawa A, Matsuzaki H and Okamoto H 2011 *Phys. Rev. B* **83** 165408
[13] Sheng Z G, Nakamura M, Koshibae W, Makino T, Tokura Y and Kawasaki M 2014 *Nat. Commun.* **5** 584
[14] Guo R, Wang Z, Zeng S, Han K, Huang L, Schlom D G, Venkatesan T, Ariando and Chen J 2015 *Sci. Rep.* **5** 12576
[15] Chong C W, Hsu D, Chen W C, Li C C, Lin J G, Chen L C, Chen K H and Chen Y F 2012 *J. Phys. Chem. C* **116** 21132
[16] Chong C W, Huang M J, Han H C, Lin Y K, Chiu J M, Huang Y F, Lin H J, Pi T W, Lin J G, Chen L C, Chen K H and Chen Y F 2013 *Appl. Phys. Lett.* **103** 211606
[17] Steinert M, Acker J, Oswald S and Wetzig K 2007 *J. Phys. Chem. C* **111** 2133
[18] Zhu J, Zhang H, Zhang P X, Xie K and Hu J T 2010 *Acta Phys. Sin.* **59** 6417 (in Chinese)
[19] Boschker H, Mathews M, Houwman E, Nishikawa H, Vailionis A, Koster G, Rijnders G and Blank D 2009 *Phys. Rev. B* **79** 214425
[20] Nishikawa H, Houwman E, Boschker H, Mathews M, Blank D and Rijnders G 2009 *Appl. Phys. Lett.* **94** 042502
[21] Vailionis A, Boschker H, Siemons W, Houwman E, Blank D, Rijnders G and Koster G 2011 *Phys. Rev. B* **83** 064101
[22] Zhou X Y, Miao J, Dai J Y, Chan H L W, Choy C L, Wang Y and Li Q 2007 *Appl. Phys. Lett.* **90** 012902
[23] Lee D B 1969 *J. Appl. Phys.* **40** 4569
[24] Bean K E 1978 *IEEE Trans. Electron Dev.* **25** 1185
[25] Seidel H, Csepregi L, Heuberger A and Baumgärtel H 1990 *J. Electrochem. Soc.* **137** 3612
[26] Evans J, Thiel P and Bartelt M 2006 *Surf. Sci. Rep.* **61** 1
[27] De K, Patra M, Majumdar S and Giri S 2007 *J. Phys. D. Appl. Phys.* **40** 7614
[28] Prasad R, Singh M P, Prellier W, Siwach P K, Rawat R, Kaur A and Singh H K 2009 *Phys. Status Solidi B* **246** 1662
[29] Kumar D, Sankar J, Narayan J, Singh R K and Majumdar A K 2002 *Phys. Rev. B* **65** 094407
[30] Hinz A P, Kettemann S and Mucciolo E R 2014 *Phys. Rev. B* **89** 075411
[31] Efros A L and Shklovskii B I 1975 *J. Phys. C: Solid State Phys.* **8** L49
[32] Baranovskii S D, Efros A L, Gelmont B L and Shklovskii B I 1979 *J Phys. C: Solid State Phys.* **12** 1023
[33] Zhang J and Shklovskii B I 2004 *Phys. Rev. B* **70** 115317
[34] Middleton A A and Wingreen N S 1993 *Phys. Rev. Lett.* **71** 3198
[35] Averin D V and Nazarov Y V 1990 *Phys. Rev. Lett.* **65** 2446
[36] Beloborodov I S, Lopatin A V and Vinokur V M 2005 *Phys. Rev. B* **72** 125121
[37] Beloborodov I S, Lopatin A V, Vinokur V M and Efetov K B 2007 *Rev. Mod. Phys.* **79** 469
[38] Tran T B, Beloborodov I S, Lin X M, Bigioni T P, Vinokur V M and Jaeger H M 2005 *Phys. Rev. Lett.* **95** 076806